Supplementary Material

$Cu_{0.5}Ni_{0.5}Fe_2O_4$@Lys-GO: A versatile heterogeneous nanocatalyst for synthesis of oxazolo heterocyclic scaffolds via a tandem oxidative cyclization pathway

Divya Jat,[a] Ashok Kumar,[a] Gunadhor Singh Okram,[b] and Pratibha Sharma[a,] *

a. School of Chemical Sciences, Devi Ahilya University, Indore 452001 (M.P.), India

b. UGC-DAE Consortium for Scientific Research, University Campus, Khandwa Road, Indore, Madhya Pradesh 452001, India.

Email: profpratibhasharma@gmail.com

Table of Contents

Figure S1. The ^{1}H NMR Spectrum of *5,5-dimethyl-2-phenyl-7H-[1,3]dioxino[5,4-d]oxazol-7-one. (***3a***):*

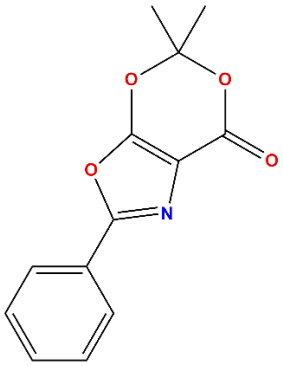

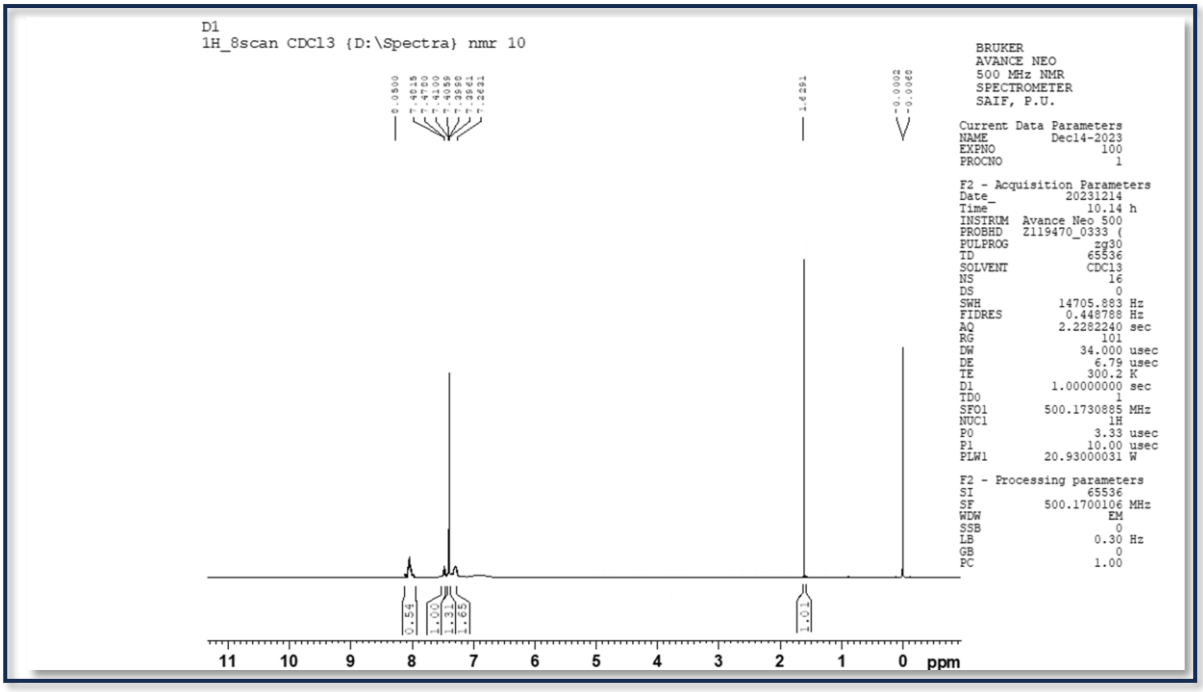

Figure S2. The ^{13}C NMR Spectrum of *5,5-dimethyl-2-phenyl-7H-[1,3]dioxino[5,4-d]oxazol-7-one. (**3a**):*

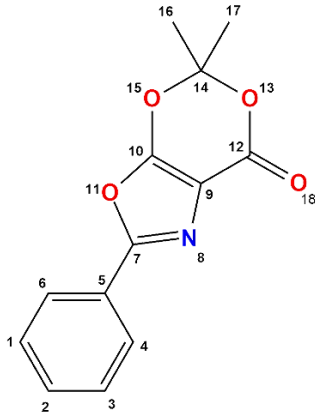

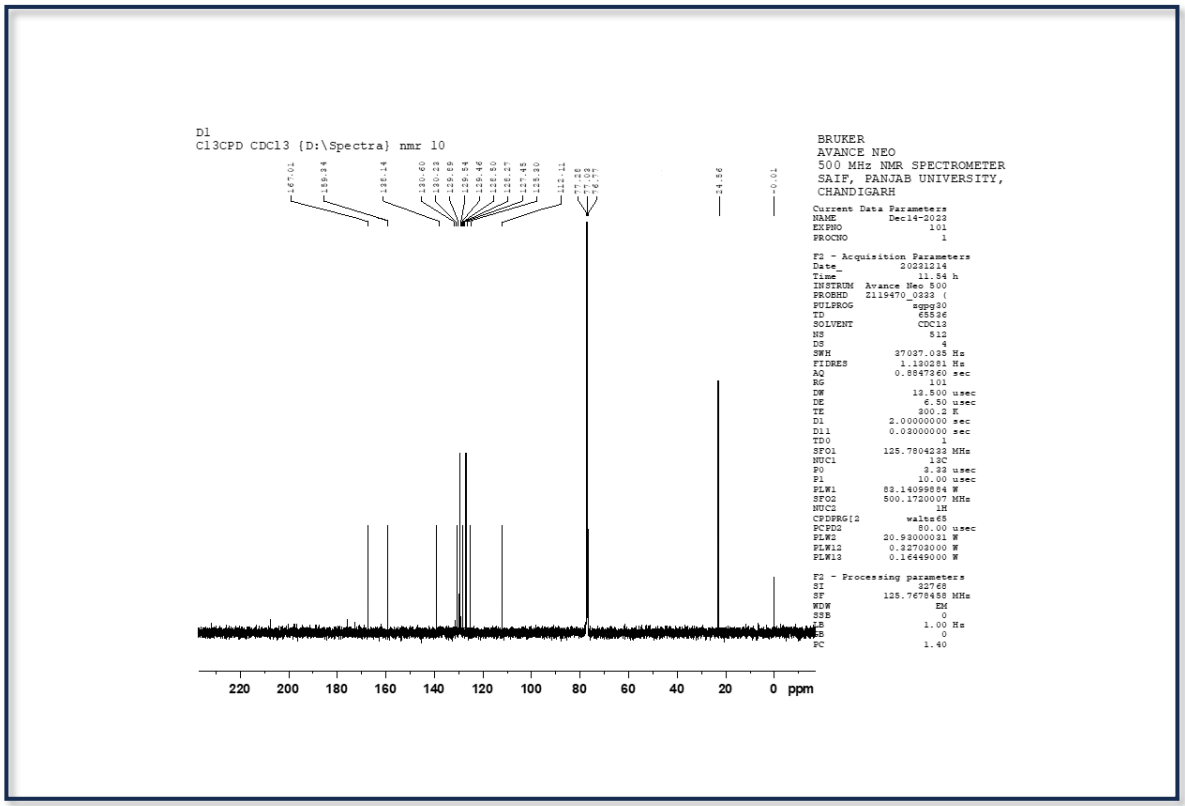

Figure S3. The ^{1}H NMR Spectrum of *5,5-dimethyl-2-(p-tolyl)-7H-[1,3]dioxino[5,4-d]oxazol-7-one. (**3b**):*

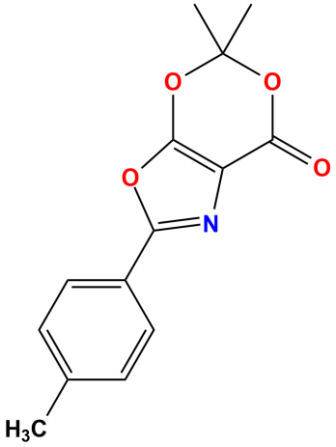

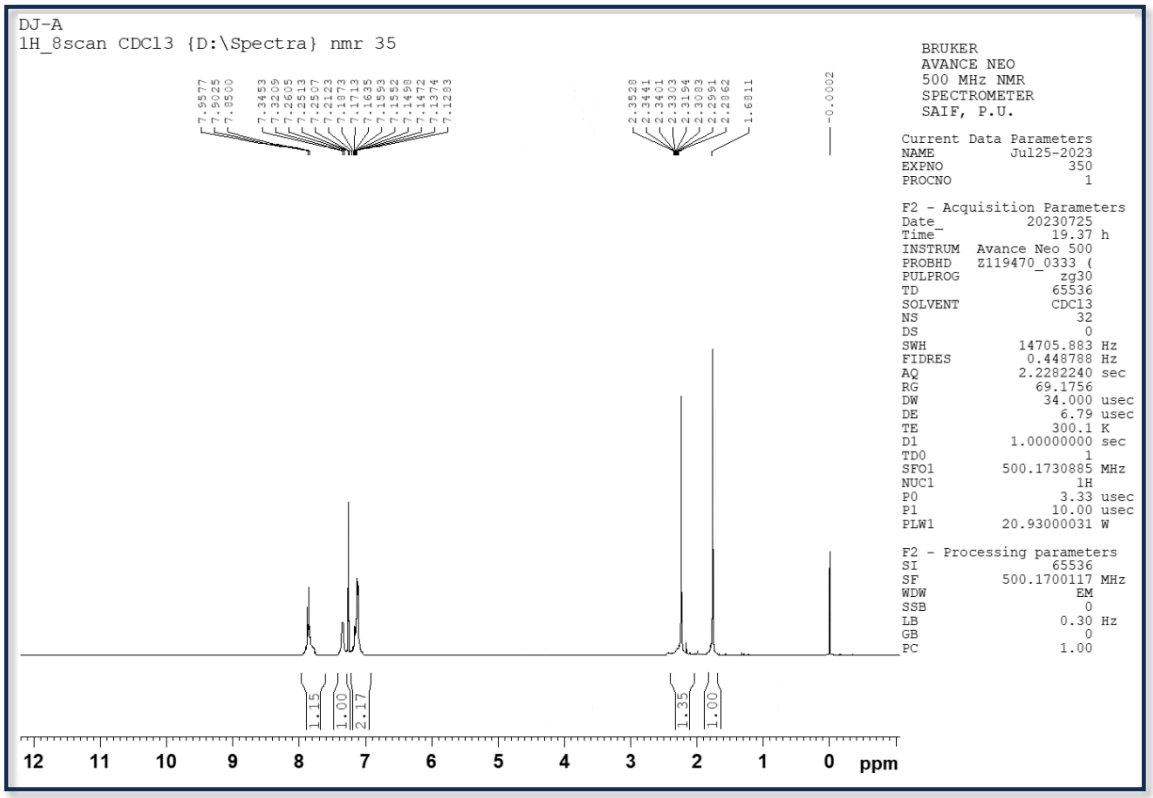

Figure S4. The ^{13}C NMR Spectrum of *5,5-dimethyl-2-(p-tolyl)-7H-[1,3]dioxino[5,4-d]oxazol-7-one. (**3b**):*

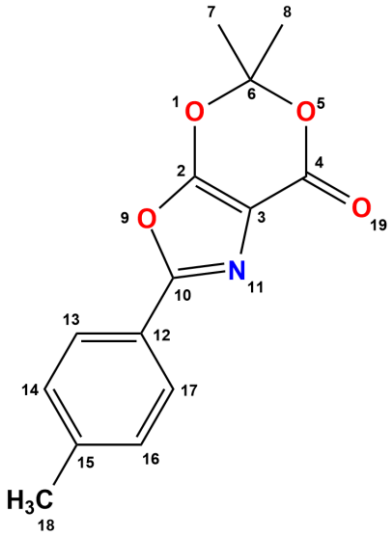

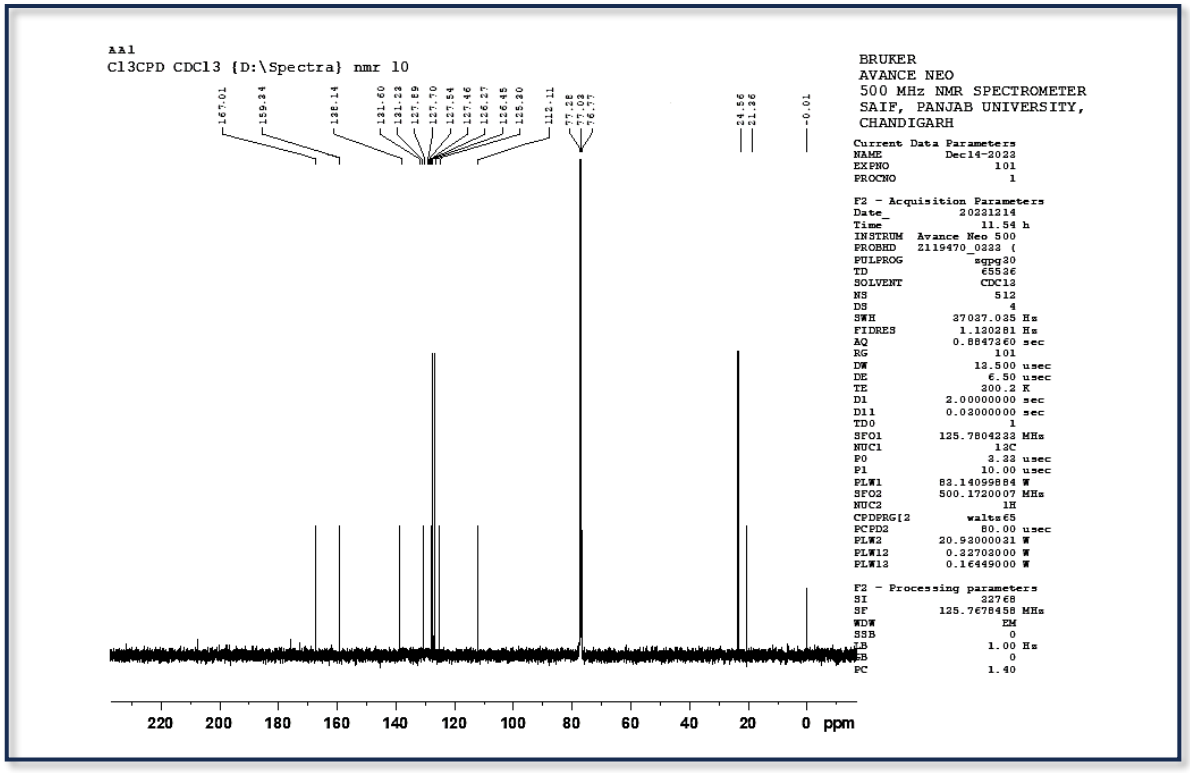

Figure S5. The ^{1}H NMR Spectrum of *2-(2-chlorophenyl)-5,5-dimethyl-7H-[1,3]dioxino[5,4-d]oxazol-7-one. (**3c**):*

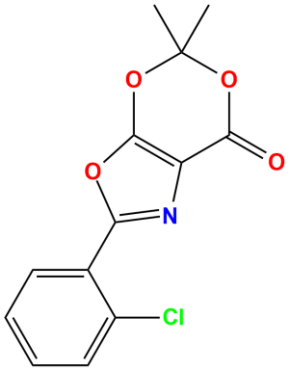

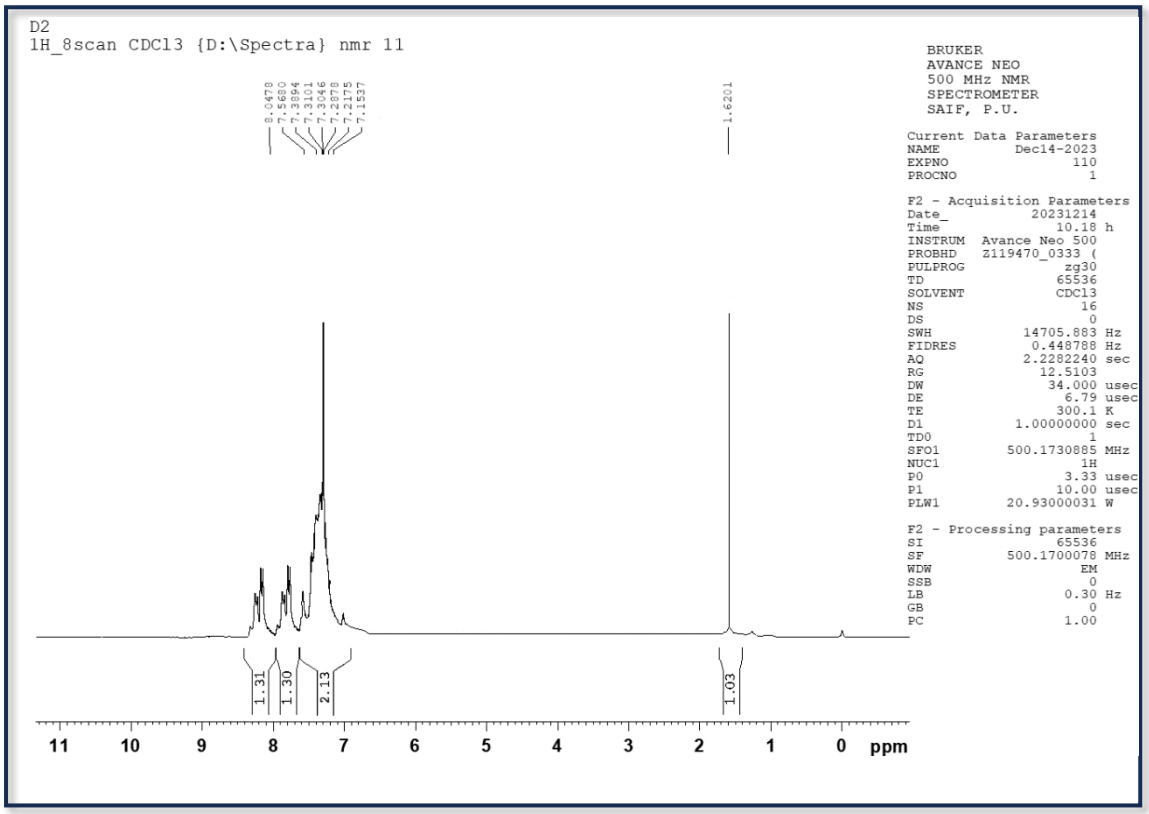

Figure S6. The ^{13}C NMR Spectrum of *2-(2-chlorophenyl)-5,5-dimethyl-7H-[1,3]dioxino[5,4-d]oxazol-7-one. (**3c**):*

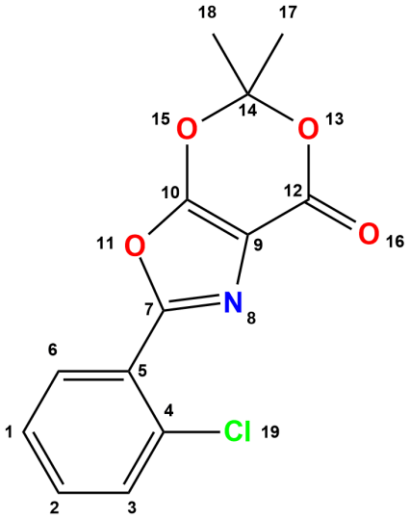

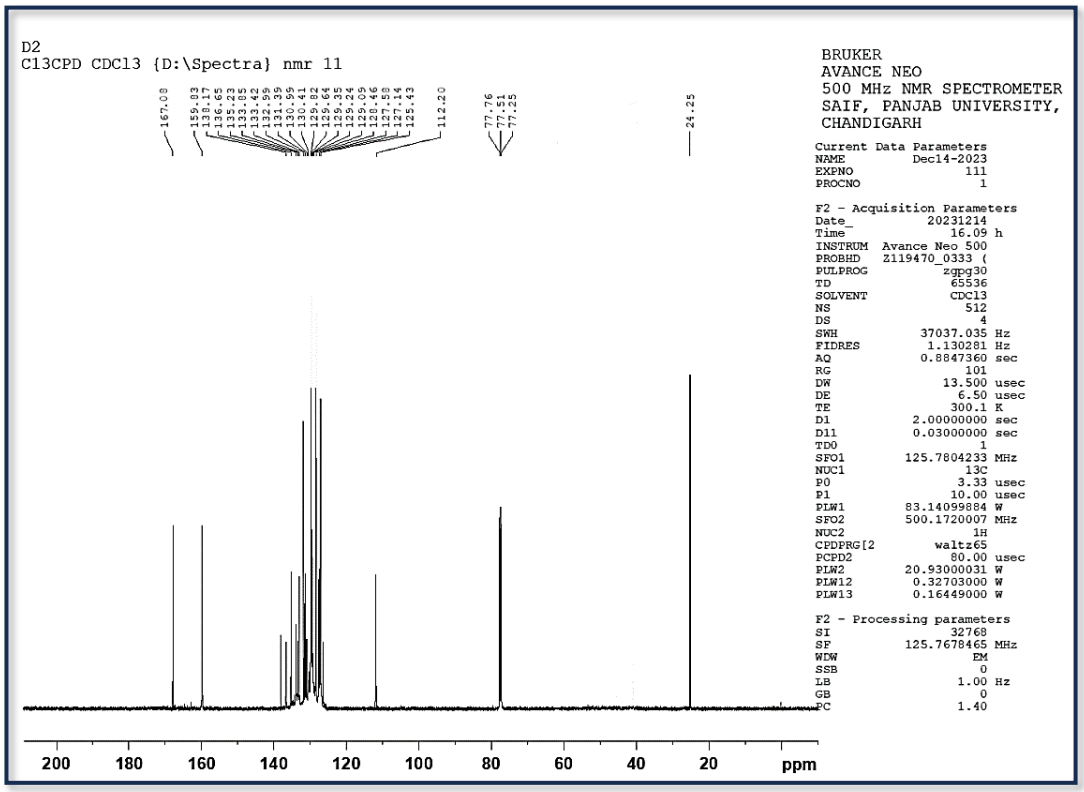

Figure S7. The ^{1}H NMR Spectrum of *2-(4-methoxyphenyl)-5,5-dimethyl-7H-[1,3]dioxino[5,4-d] oxazol-7-one. (**3d**):*

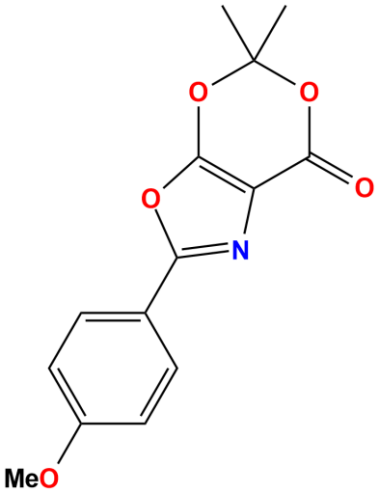

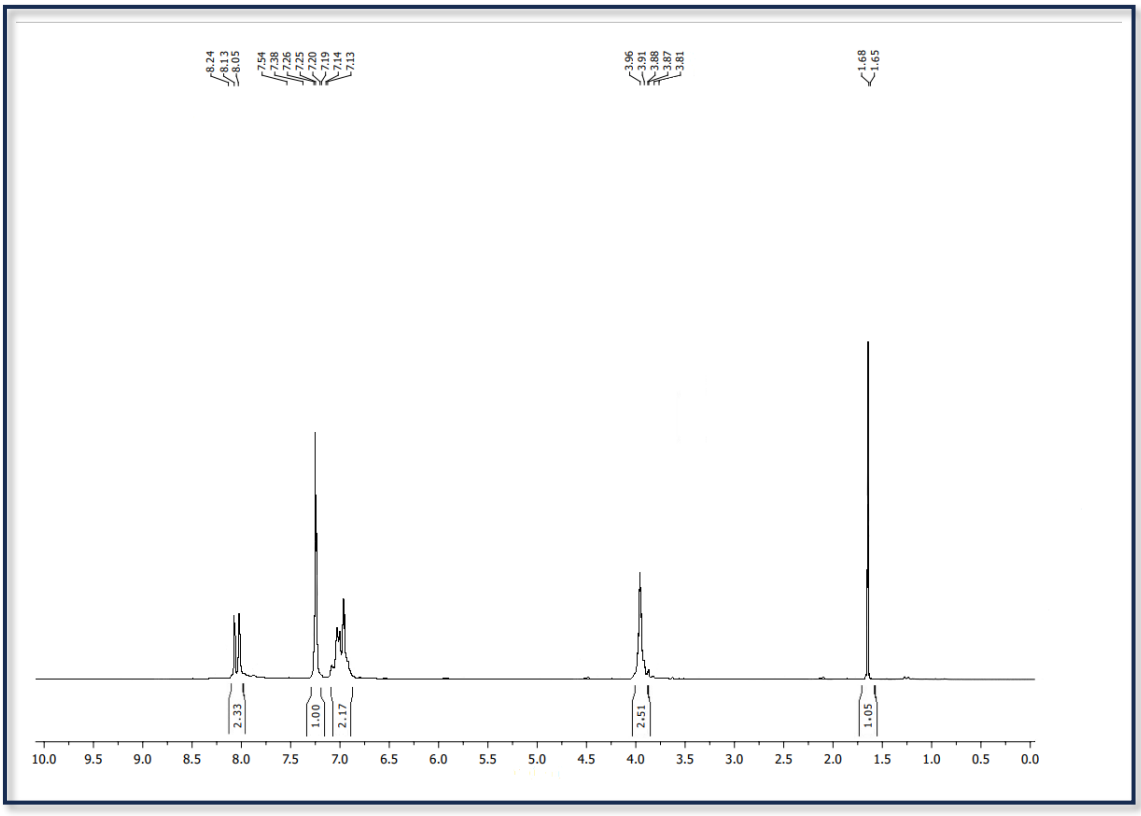

Figure S8. The ^{13}C NMR Spectrum of *2-(4-methoxyphenyl)-5,5-dimethyl-7H-[1,3]dioxino[5,4-d] oxazol-7-one. (**3d**):*

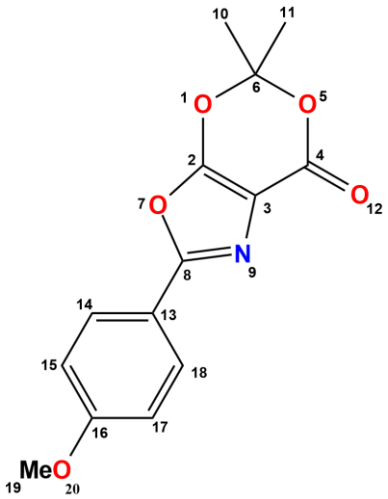

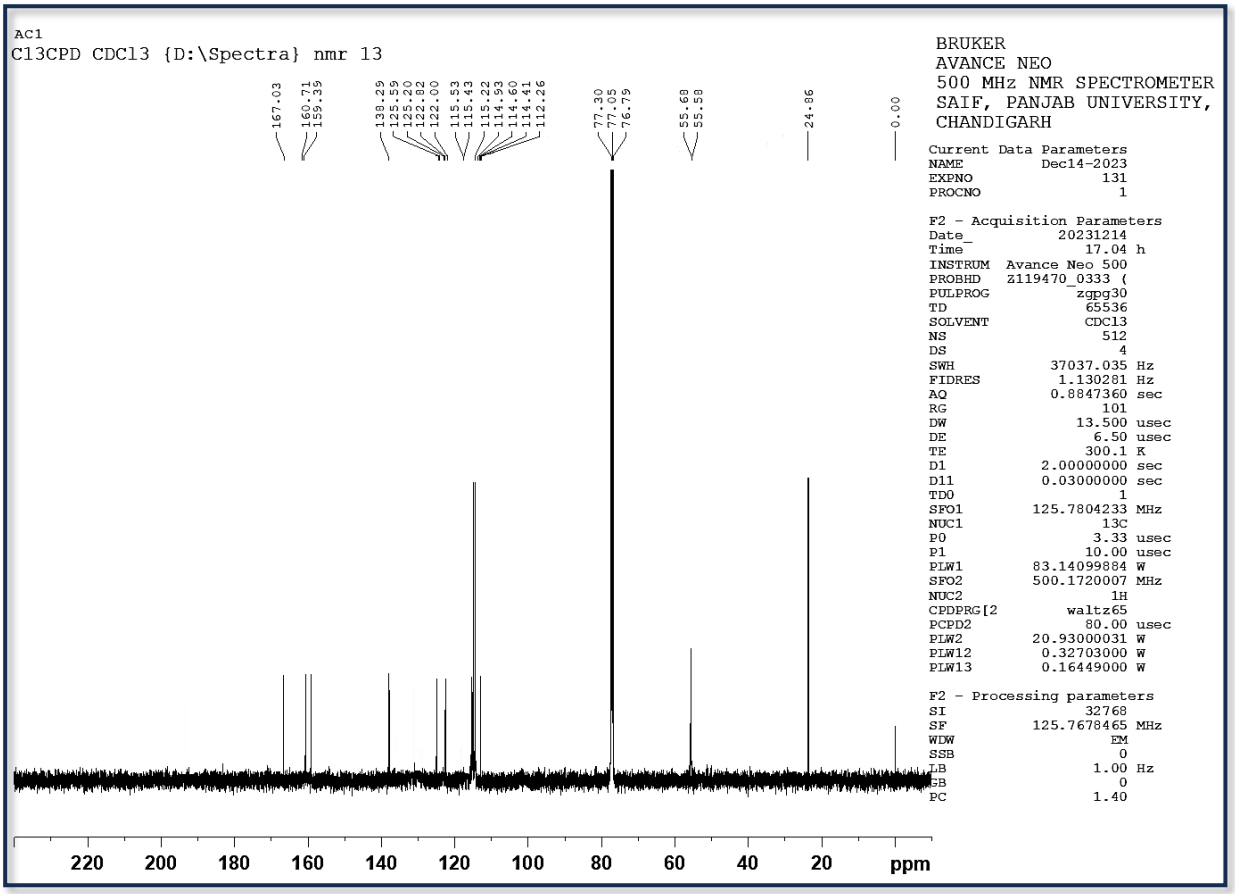

Figure S9. The ^{1}H NMR Spectrum of *6,6-dimethyl-2-phenyl-6,7-dihydrobenzo[d]oxazol-4(5H)-one. (**3e**):*

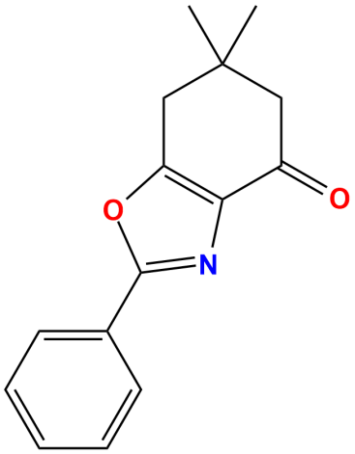

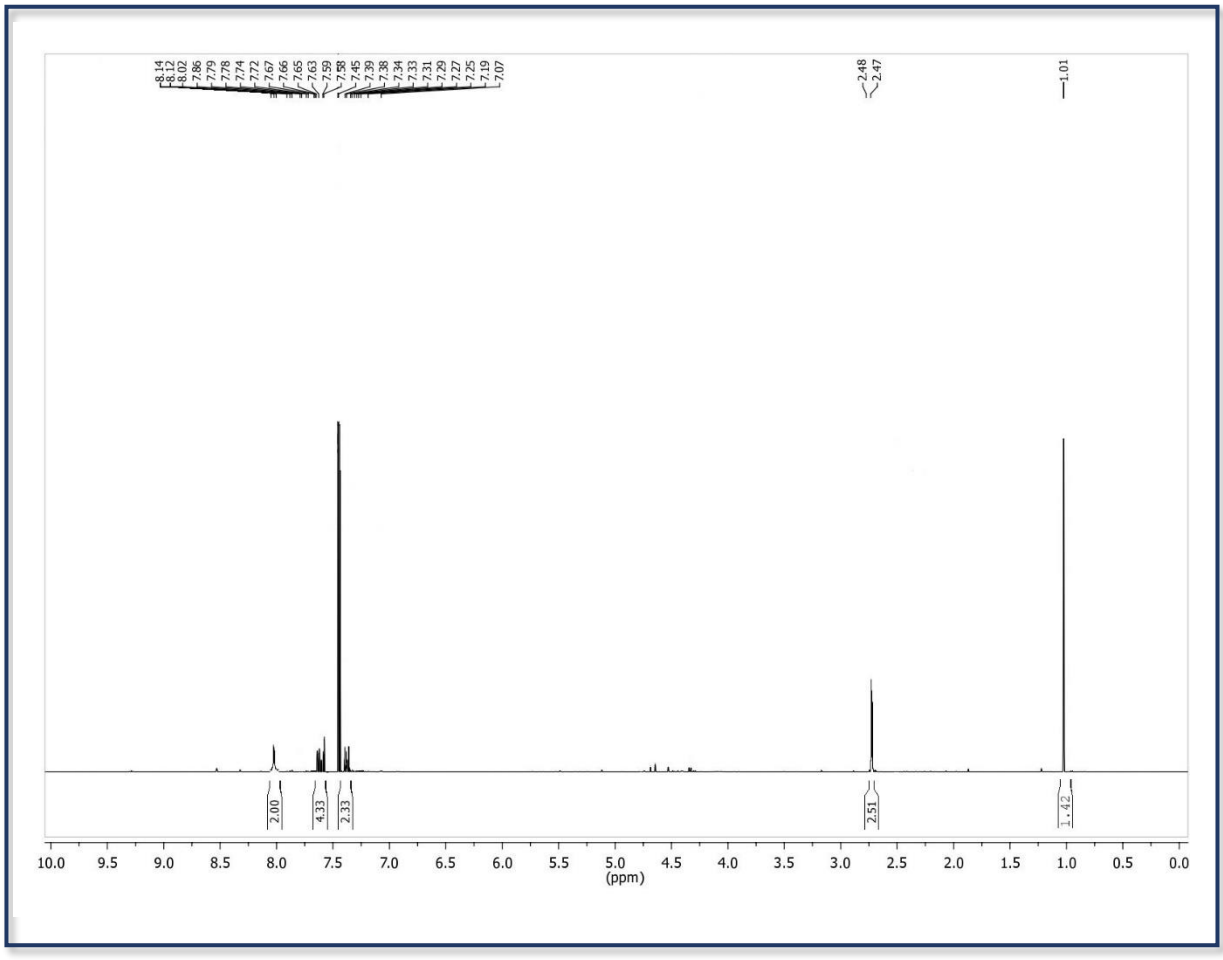

Figure S10. The ^{13}C NMR Spectrum of *6,6-dimethyl-2-phenyl-6,7-dihydrobenzo[d]oxazol-4(5H)-one. (**3e**):*

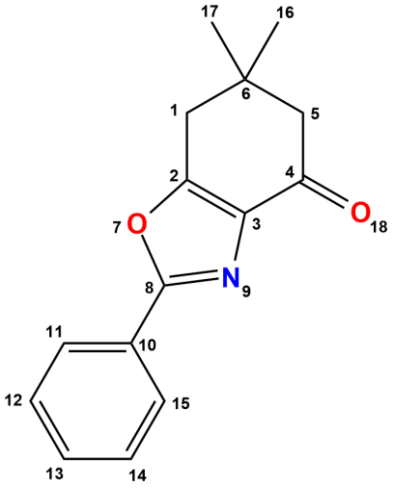

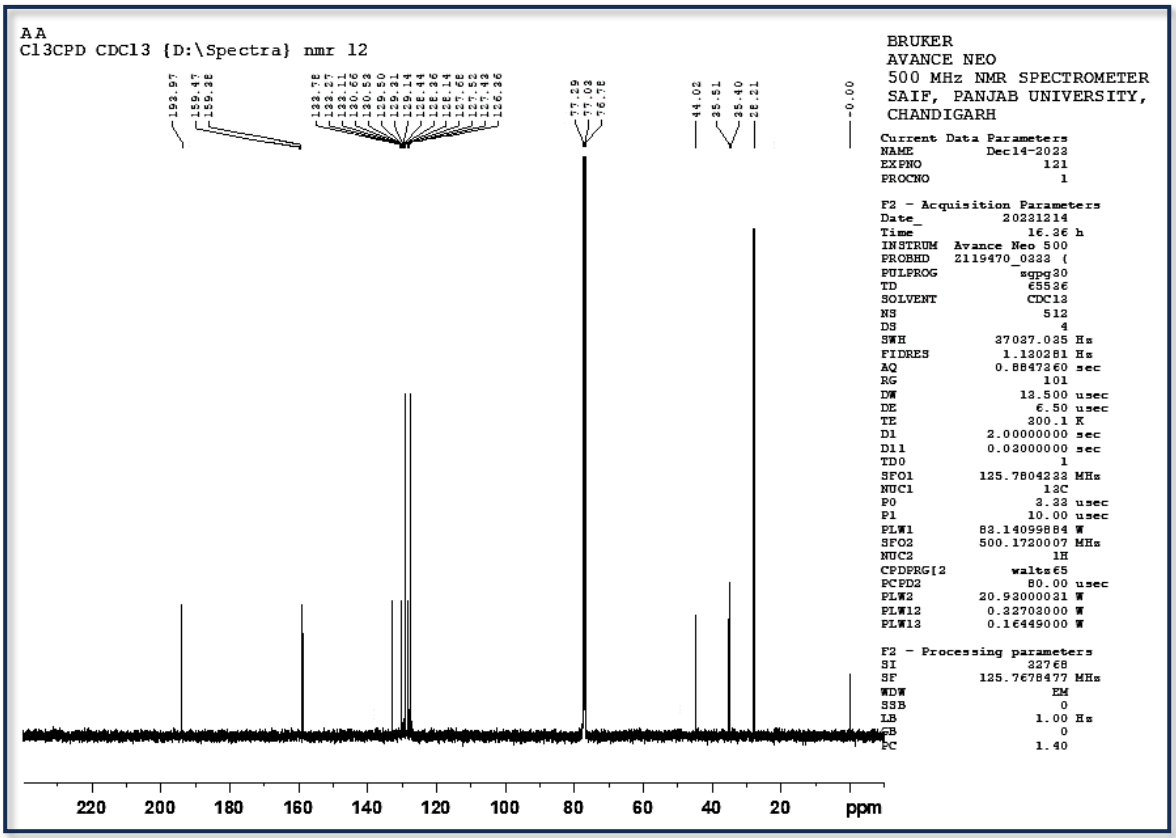

Figure S11. The ^{1}H NMR Spectrum of *6,6-dimethyl-2-(p-tolyl)-6,7-dihydrobenzo[d]oxazol-4(5H)-one. (**3f**):*

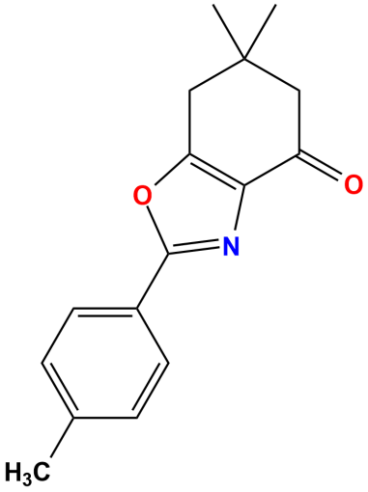

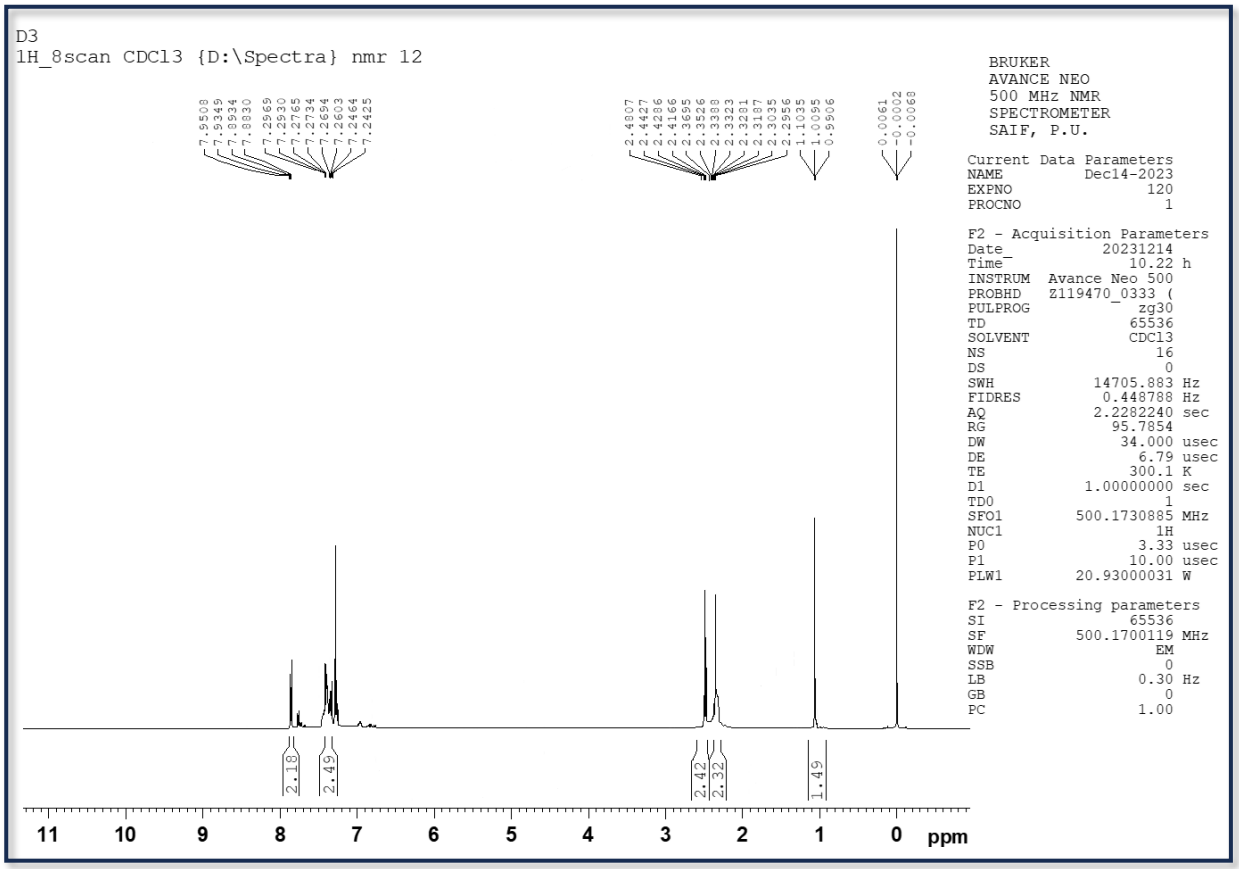

Figure S12. The ^{13}C NMR Spectrum of *6,6-dimethyl-2-(p-tolyl)-6,7-dihydrobenzo[d]oxazol-4(5H)-one. (**3f**):*

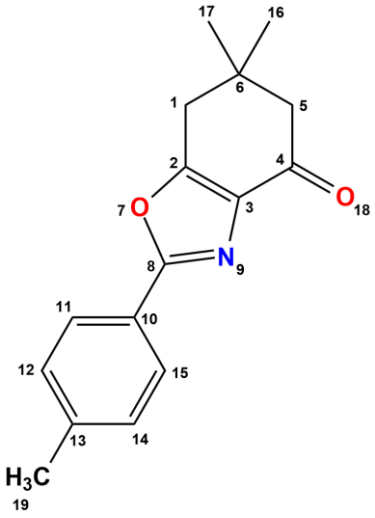

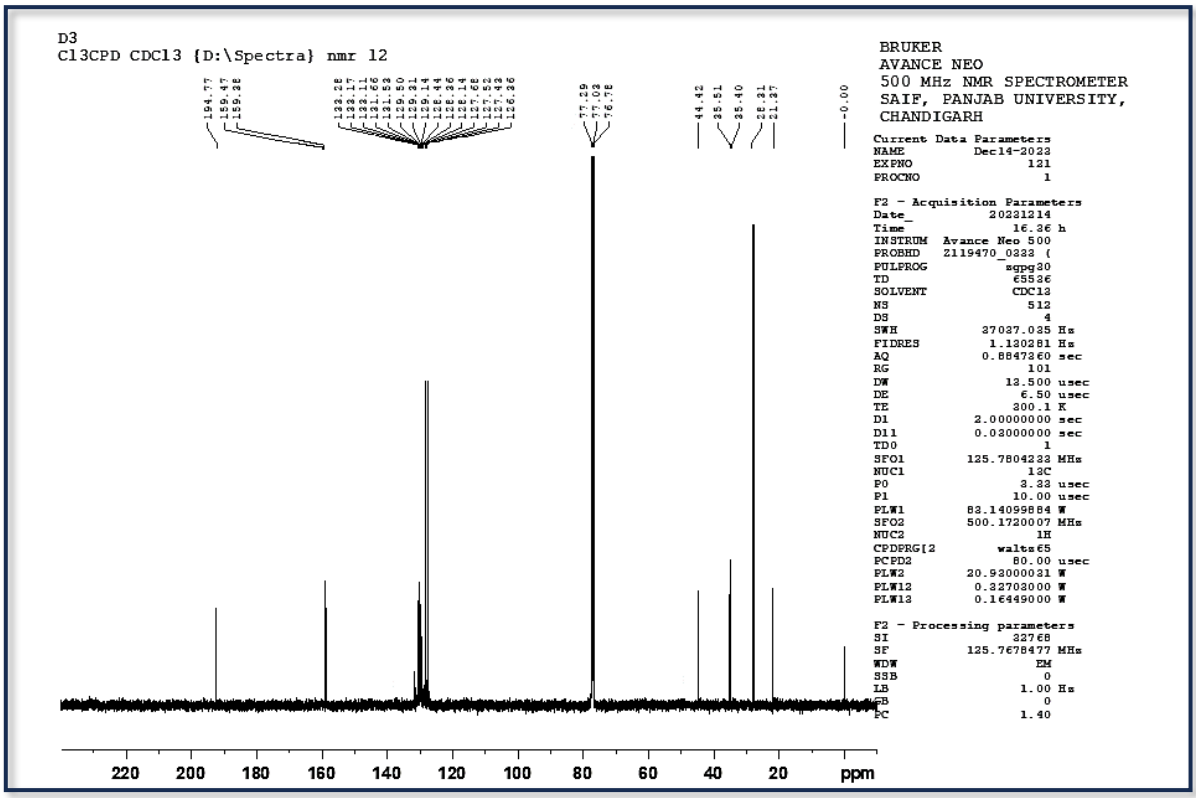

Figure S13. The ^{1}H NMR Spectrum of *2-(2-chlorophenyl)-6,6-dimethyl-6,7-dihydrobenzo[d]oxazol-4(5H)-one. (**3g**):*

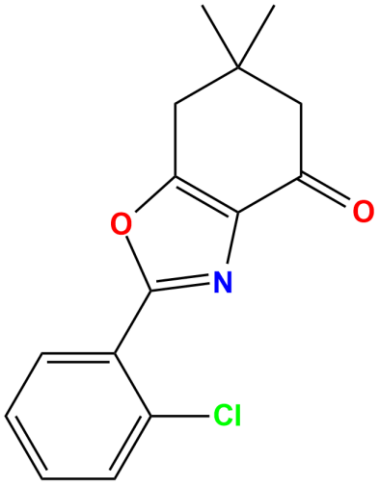

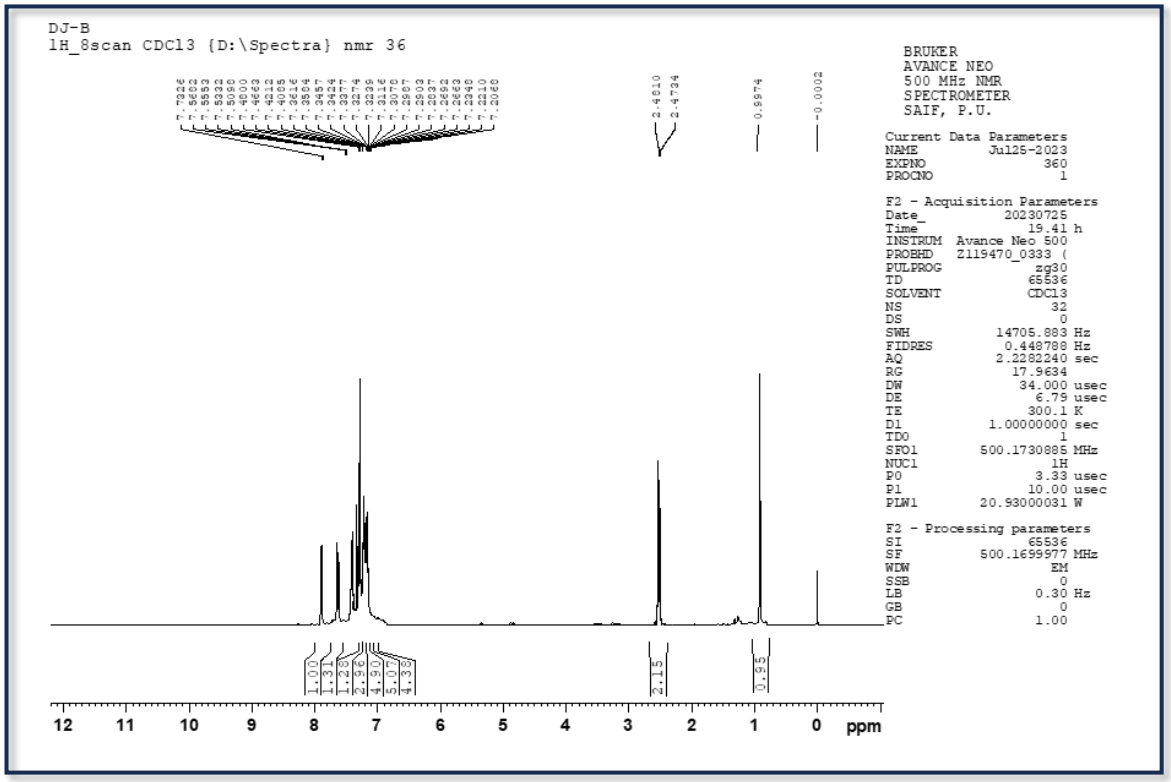

Figure S14. The ^{13}C NMR Spectrum of *2-(2-chlorophenyl)-6,6-dimethyl-6,7-dihydrobenzo[d]oxazol-4(5H)-one. (**3g**):*

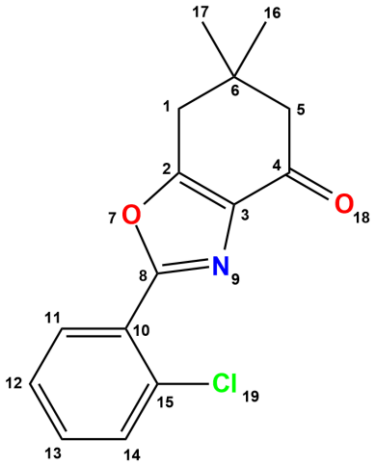

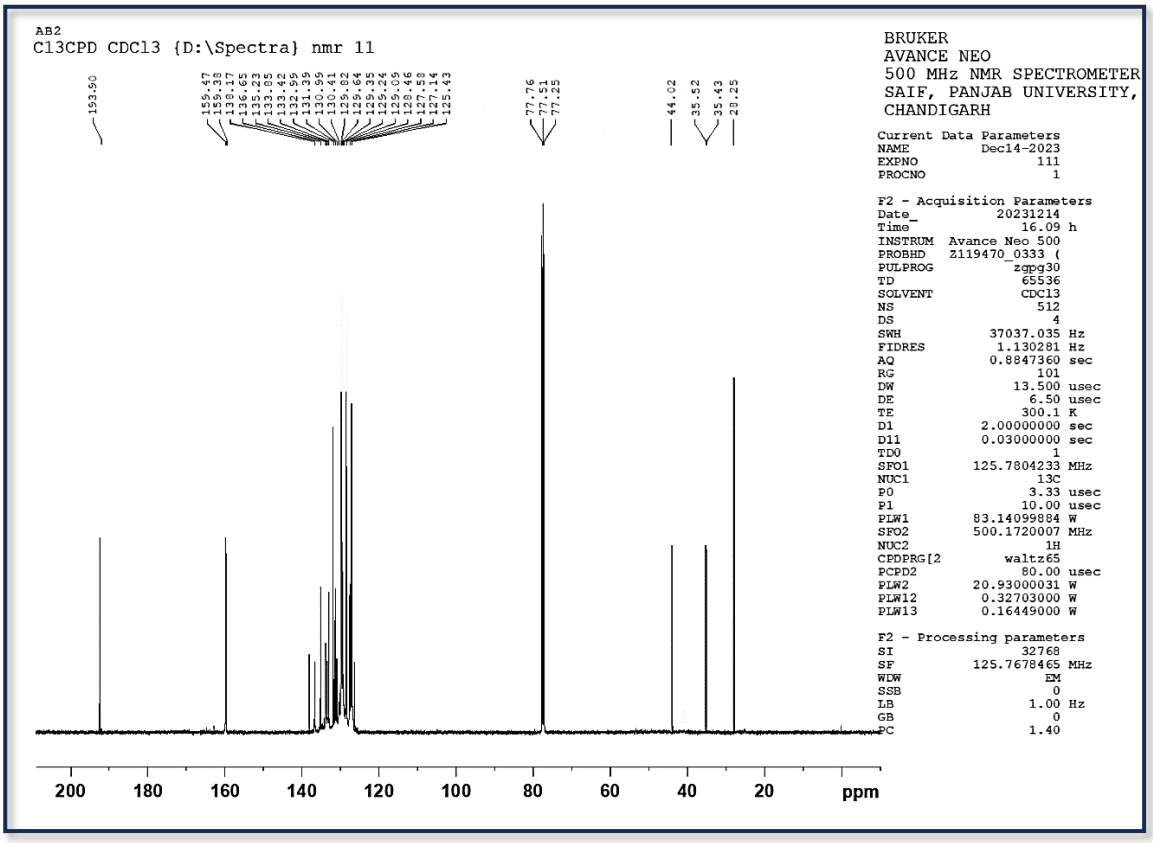

Figure S15. The ^{1}H NMR Spectrum of *2-(4-methoxyphenyl)-6,6-dimethyl-6,7-dihydrobenzo[d]oxazol-4(5H)-one. (**3h**):*

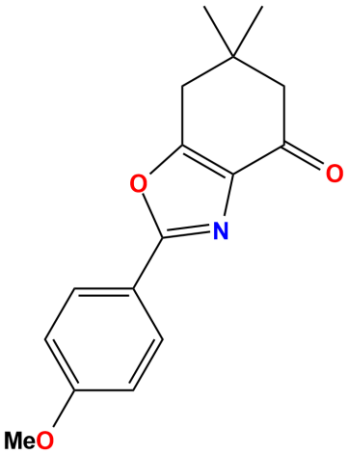

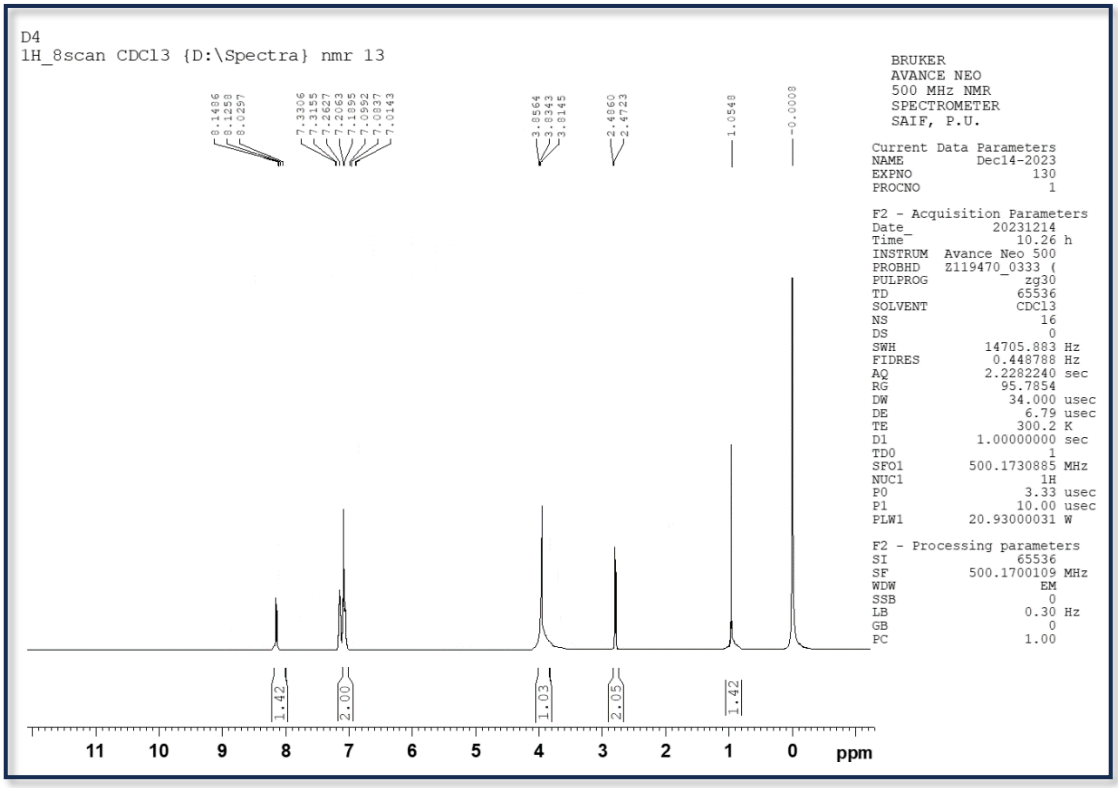

Figure S16. The ^{13}C NMR Spectrum of *2-(4-methoxyphenyl)-6,6-dimethyl-6,7-dihydrobenzo[d]oxazol-4(5H)-one. (**3h**):*

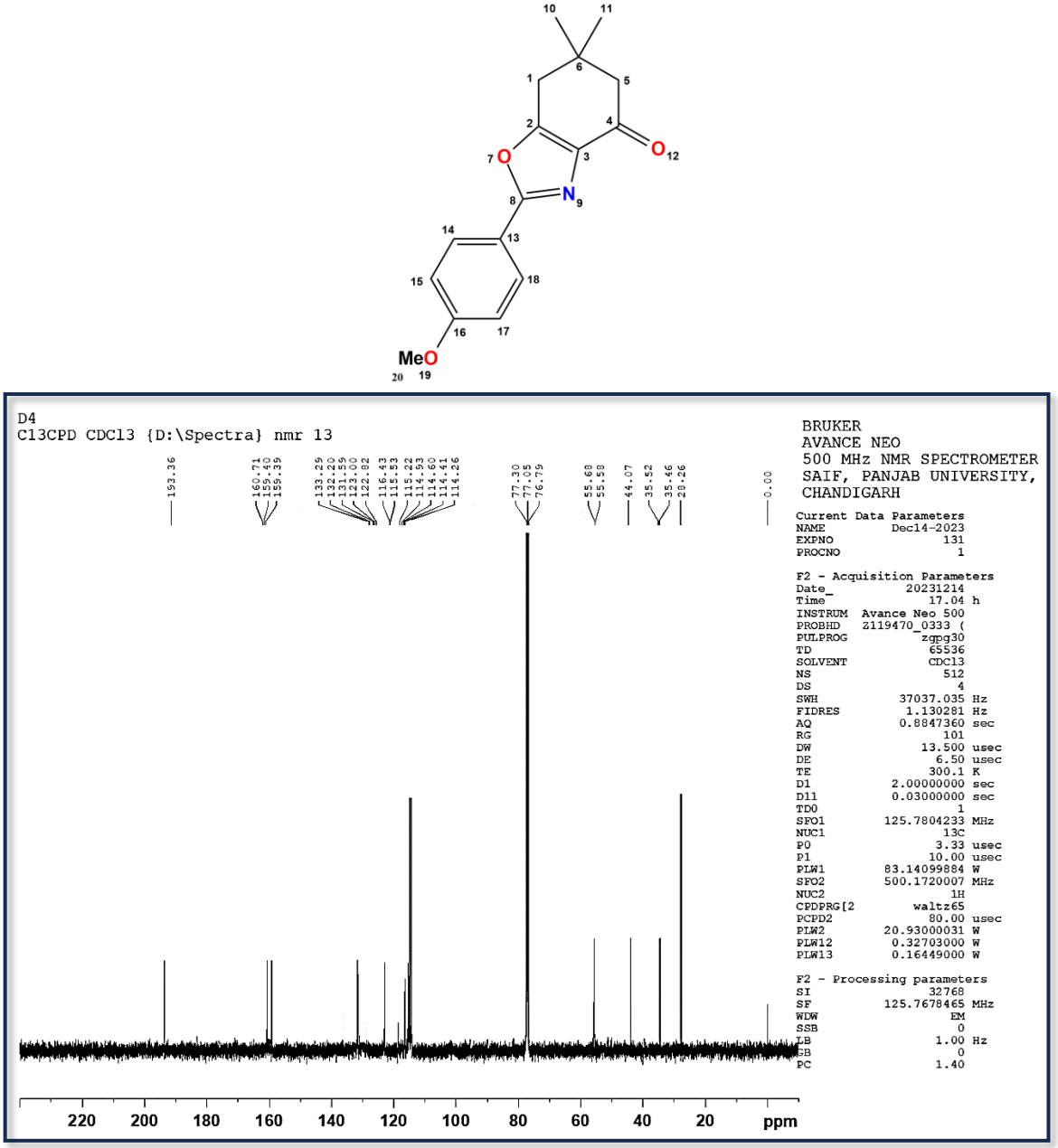

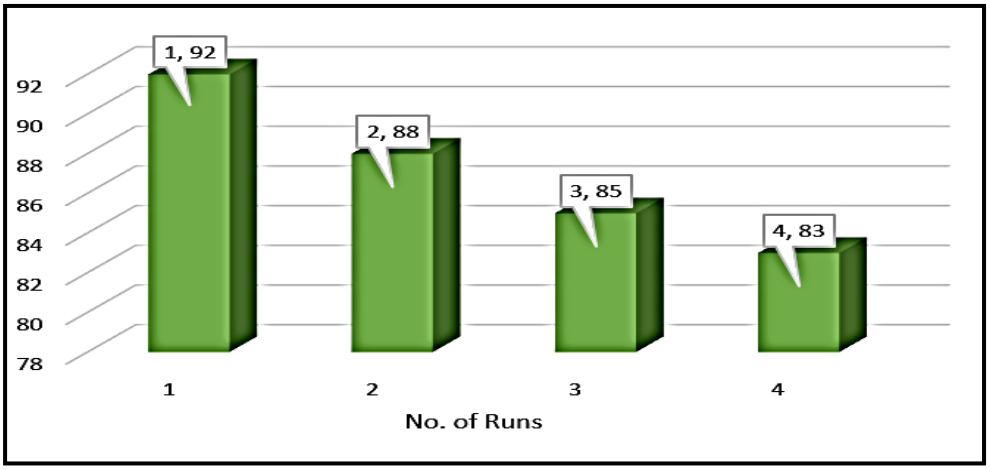

Figure S17. Recycle and reusability of magnetic $Cu_{0.5}Ni_{0.5}Fe_2O_4$@Lys-GO

Table S1. Ecoscale calculation for the reaction of Benzylamine, Meldrum's acid, I_2, and H_2O_2 in the presence of Methanol.

ECOSCALE PENALTY POINTS	DETAILS OF PARAMETER	PENALTY POINTS[b]
1. YIELD		4
2. COST OF REACTANTS	Benzylamine	0
	Meldrum's acid	0
	I_2	0
	H_2O_2	0
	Methanol	
	$Cu_{0.5}Ni_{0.5}Fe_2O_4$@Lys-GO	0
3. SAFETY[a]	Benzylamine (T)	5
	Meldrum's acid (T)	5
	I_2 (T)	5
	H_2O_2 (T)	5
	Methanol	0
	$Cu_{0.5}Ni_{0.5}Fe_2O_4$@Lys-GO	0
4. TECHNICAL SETUP	Common Setup	0
5. TEMPERATURE/TIME	Room temperature, < 24h	1
6. WORKUP AND PURIFICATION	Adding solvent	0
TOTAL PENALTY POINTS		25

[a]Based on the hazard warning symbols.

[b]The total of all penalties was 25, which gave a score of **75** (100 - 25), which is indicative of anacceptable green synthesis.

Calculation of E-factor, mass intensity, atom economy, reaction mass efficiency, and carbon efficiency for the reaction of 2-chloro benzylamine and Meldrums acid in the presence of methanol.

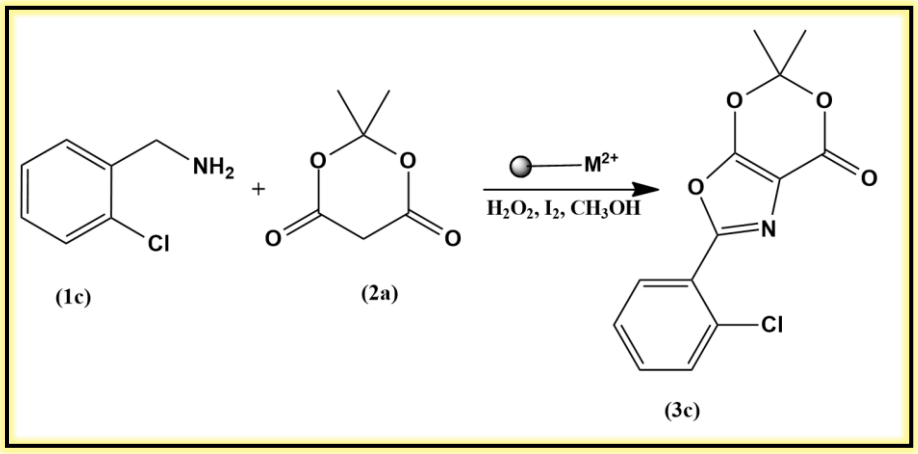

- **Total amount of reactants**: Reactant (1c) + Reactant (2*a*) = 0.141g + 0.144g = **0.285g**
- **Amount of final product (3a)**: **0.279 g**
- **Amount of waste:** (0.285g – 0.279g) = 0.006g

$$\boldsymbol{E\ factor = \frac{Amount\ of\ Waste}{Amount\ of\ Product}}$$

$$\boldsymbol{E\ factor = \frac{0.006g}{0.279g}}$$

$$E\ factor = 0.0215$$

- **Process Mass Intensity (PMI)**

$$Process\ Mass\ Intensity = \frac{Amount\ of\ Waste + Amount\ of\ Product}{Amount\ of\ Product}$$

$$Process\ Mass\ Intensity = E - Factor + 1$$

$$Process\ Mass\ Intensity = 1.0215$$

- **Atom Economy (AE)**

$$Atom\ Economy = \frac{MW\ of\ desired\ Product}{\Sigma\ of\ MW\ of\ stoichiometric\ reactant}\ x\ 100$$

$$Atom\ Economy = \frac{279.68}{285.73}\ x\ 100$$

$$Atom\ Economy = 97.88\ \%$$

- **Reaction Mass Efficiency**

$$\boldsymbol{Reaction\ Mass\ Efficiency = \frac{Mass\ of\ desired\ Product}{\Sigma\ of\ Mass\ of\ reactant}\ x\ 100}$$

$$\boldsymbol{Reaction\ Mass\ Efficiency = \frac{0.252}{0.285}\ x\ 100}$$

$$\boldsymbol{Reaction\ Mass\ Efficiency = 88.4\ \%}$$

Table S2. Influence of additives on tandem oxidative cyclization of amines and 1,3 dicarbonyls

Entry	Additive	Conversion %[b]
1.	No additive	47
2.	NIS	72
3.	I_2	92
4.	KI	56
5.	TBAI	51
6.	NBS	50

[a] Reaction conditions: Meldrum's acid (1 mmol), benzylamine (2 mmol), $CuNiFe_2O_4$@Lys-GO catalyst (30 mg), H_2O_2 (2 mmol), additive (1.2 mmol), CH_3OH (3 mL), 3h; [b] Conversion percentages determined via GC-MS

Characterization of Nanocatalysts

Powder X-ray diffraction (PXRD) analyses.

X-ray diffraction (PXRD) was conducted to characterize the structural properties of graphene oxide, Lys-GO, and Lys-GO decorated with $CuNiFe_2O_4$ magnetic nanoparticles ($CuNiFe_2O_4$) as shown in Figure S18. The average crystallite diameter (D) was estimated by utilizing the Debye-Scherrer equation.

$$D = \frac{K\lambda}{\beta \cos\theta}$$

Where D is the average crystallite size, K is the particle shape factor whose value is 0.9, λ is the X-ray wavelength of Cu-Kα radiations (1.54056Å), θ is the Bragg's angle of the radians and β is the e line broadening at full width at half maximum (FWHM) of a diffracted peak[1]. Accordingly, the average crystallite size of the Lysine grafted graphene oxide decorated with copper-substituted nickel ferrite nanoparticle was obtained from the abovementioned equation and found to be 11-15 nm. To examine the X-ray diffraction data, we used JADE (Joint Automated Data Evaluation) to analyze X-ray diffraction data and utilize the JCPDS database (JCPDS 00-010-0325) for peak matching and detection, as shown in Figure S18. The parent graphite displayed a distinctive sharp peak at 26.7° concerning the plane with an interlayer spacing equal to 0.33 nm. Following graphite's oxidation to graphene oxide, the resulting GO exhibits the diffraction peak at 2θ = 11.36° with an interlayer spacing value of 0.74 nm which was attributed to the intercalation with water and oxygen-containing functional groups between the basal plane of the graphite[2]. There is an incomplete oxidation of graphite to graphene oxide which is corroborated by the occurrence of graphite peak at 26.7° displayed in the XRD pattern. The diffraction characteristic peaks associated with the $Cu_{0.5}Ni_{0.5}Fe_2O_4$ are observable at 2θ = 16.97°, 26.60°, 38.21°, 39.45°, 46.76°, and 60.06° corresponding to the (111), (110), (220), (222), (400) and (440) were assigned to $Cu_{0.5}Ni_{0.5}Fe_2O_4$ [3].

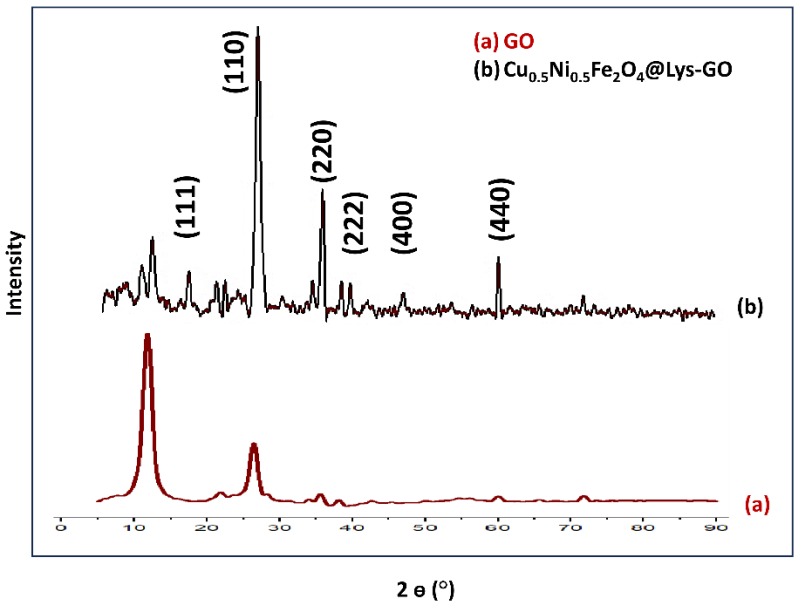

Figure S18. XRD patterns of GO (a), and Cu0.5Ni0.5Fe2O4@Lys–GO (b)

Field emission scanning electron microscope and energy-dispersive X-ray spectroscopy.

The grain size, surface morphology, and compositional findings of the catalyst were confirmed by field emission scanning electron microscope (FE-SEM) (Figure S20) with energy-dispersive X-ray spectroscopy (EDAX) (Figure S19) analyses, respectively. The SEM images of $Cu_{0.5}Ni_{0.5}Fe_2O_4$@Lys-GO have well-defined show it to be a porous network and sponge nanocomposite structure having the $Cu_{0.5}Ni_{0.5}Fe_2O_4$ nanoparticles uniformly dispersed on the lysine–grafted graphene oxide nanosheet surfaces.

EDAX survey studies authenticated the existence of vital elements in the as-prepared sample. The distinct peaks of the EDAX spectrum (Figure S19) confirmed the presence of Nickel (Ni), Copper (Cu), Iron (Fe), Oxygen (O), Nitrogen (N), and Carbon (C) being the only component in the magnetic nanoparticles.

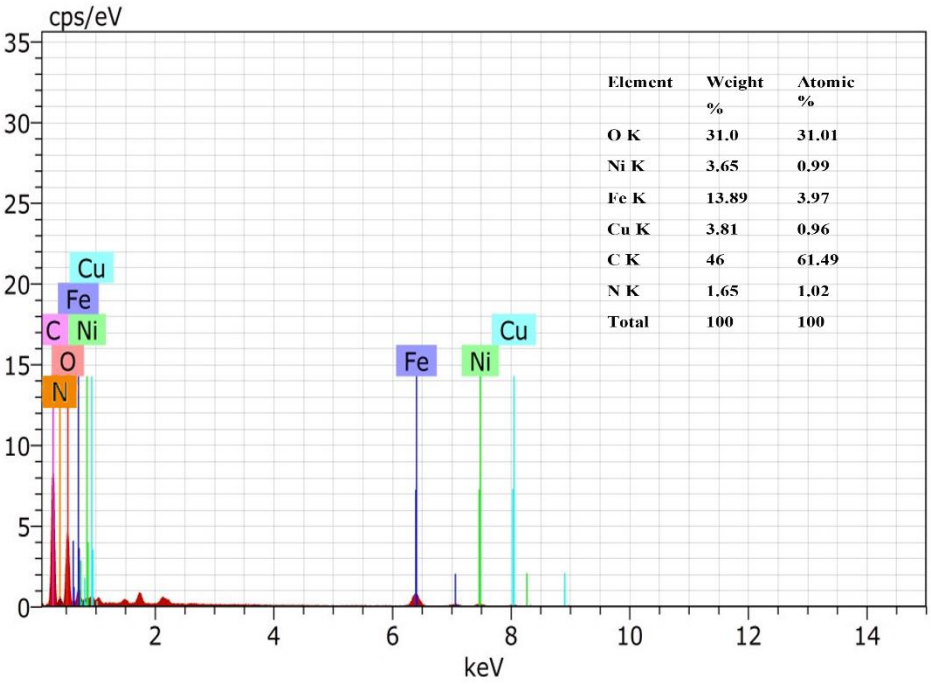

Figure S19. The EDAX pattern of Cu0.5Ni0.5Fe2O4@Lys-GO

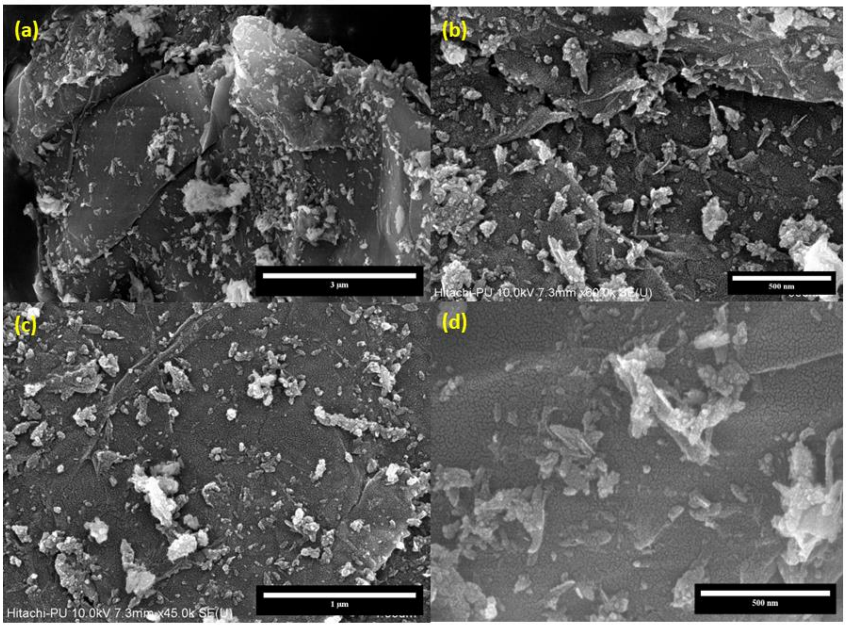

Figure S20. The field emission scanning electron microscopy (FE-SEM) images of $Cu_{0.5}Ni_{0.5}Fe_2O_4$@Lys-GO in magnification

Thermo gravimetric analyses

The thermo gravimetric analyses TGA, coupled with differential thermal analyses DTA was used to study the thermal stability decomposition profile and kinetics of synthesized Graphene oxide and $Cu_{0.5}Ni_{0.5}Fe_2O_4$@Lys-GO displayed in Figures S21 & S22 respectively. It is verified that the general decomposition occurred between the temperature ranges 25°C to 1000°C under the N_2 atmosphere followed by a weight loss process in three stages. Initially, it is attributed that the weight loss of 14.925% occurred in the temperature range of 96°-337°C,

which is corroborated by the loss of water, more specifically dehydration of crystalline adsorbed water on the catalyst surface, which can be seen in the endothermic peak in the DTA (Green line) curve. Besides, the second weight loss, associated with the evolution of CO2 of about 21.91% is in the temperature range of 337°C to 462.173°C. Consequently, lessening in the loss of mass about 12.95 % ranging between 755°C to 900°C, was observed in the decomposition of combustible organic products and amorphous hydrocarbonates, which were generated at high temperatures before the metal oxide's formation. In the range of 96°-337°C and 337°C to 462.173°C, there were two phases of significant weight loss related to the decomposition of GO and Lysine.

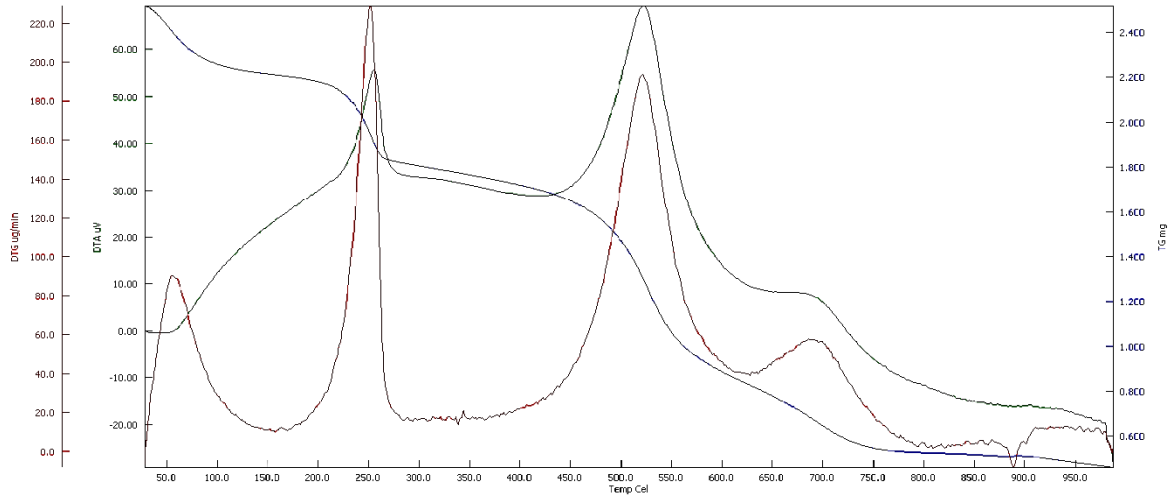

Figure S21. The TGA, DTA, and DTG patterns for Graphene Oxide

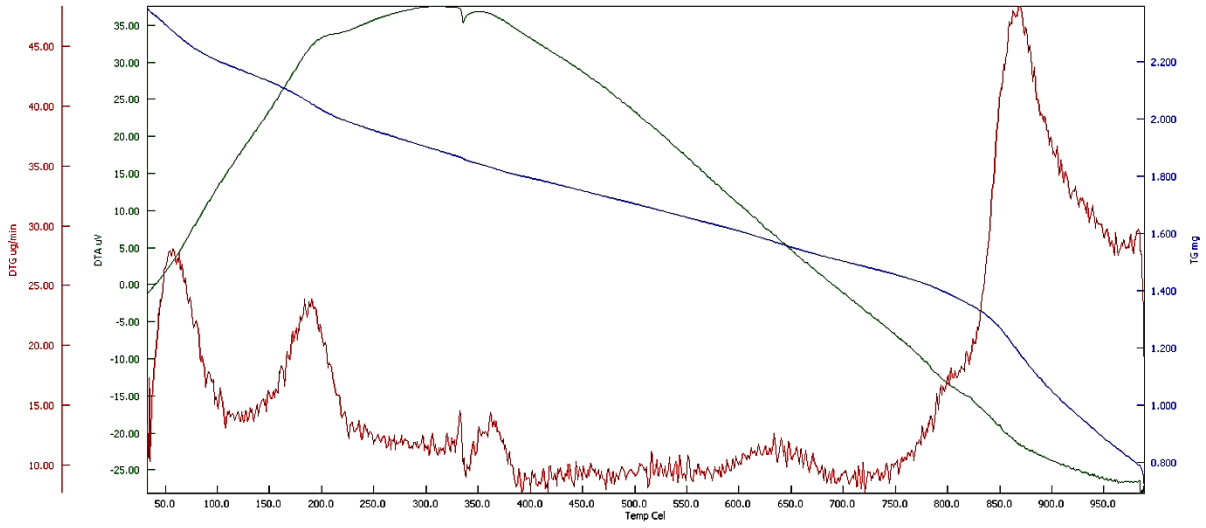

Figure S22. The TGA, DTA, and DTG patterns for Cu0.5Ni0.5Fe2O4@Lys-GO

FT-IR spectroscopy.

The FT-IR spectra were used to substantiate the functionalization of graphene oxide nanosheet by lysine amino acid and the confinement of the $Cu_{0.5}Ni_{0.5}Fe_2O_4$ nanocomposite on lysine-grafted graphene oxide. The comparative FT-IR patterns for graphene oxide, Lysine grafted graphene oxide and $Cu_{0.5}Ni_{0.5}Fe_2O_4$ immobilized on Lysine grafted graphene oxide

were also recorded as presented in Figure S23. These analyses also divulged the formation of spinel ferrites and the shifting in vibrational frequencies correspond to the exchange of cations between tetrahedral and octahedral sites.

The GO exhibits various prominent peaks as we can see in the graph the existence of hydroxyl (OH) can be confirmed by the broad peak in the high-frequency area at 3355.23 cm^{-1}, while the band observed at 1731.66 cm^{-1} is assigned to carbonyl carbon and a peak at 1621.81 cm^{-1} is observed due to presence of C=C stretching, another peak at 1223.82 cm^{-1} represents C-O-C functional group. The peak at 1044.76 cm^{-1} corresponds to the vibrational mode of the C-O group. The new characteristic bands appeared at 1624 cm^{-1} and 1408 cm^{-1} (IR spectrum of lysine-GO) corresponding to the –C=N and –C–N stretches, respectively, revealing the chemical reaction of lysine to the GO[4]. The spinel ferrite ascribed the intrinsic bands at 621 cm^{-1} assigned for the intrinsic stretching vibrations of metal-O at the tetrahedral site and 428 cm^{-1} is pronounced for octahedral-metal-O stretching in the $Cu_{0.5}Ni_{0.5}Fe_2O_4$@Lys–GO nanocomposite[5].

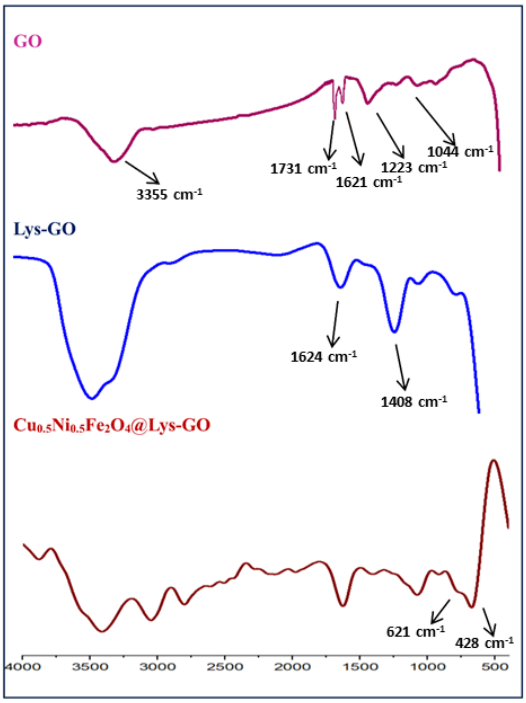

Figure S23. FTIR spectra of (a) GO, (b) Lys-GO, (c) $Cu_{0.5}Ni_{0.5}Fe_2O_4$@Lys-GO

Magnetic Properties Evaluation.

The magnetic properties of the synthesized nanocatalyst are analyzed using a Magnetometer (VSM) at room temperature under the magnetic field strength sweeping between -20,000 Oe to 20,000 Oe gradient. Figure S24, correlated to the magnetic hysteresis curves at room temperature (300K), was surveyed for the lysine grafted graphene oxide with copper-substituted nickel ferrite magnetic nanoparticle and exhibits ferromagnetic behavior at room temperature. The saturation magnetization is discovered to be 26.907 emu g^{-1}, which is more than enough for the segregation of the catalyst from the reaction mixture by applying an external magnetic field. The remanence magnetization (Mr) and the coercivity (Hc) of the

samples are 4.87 emu g^{-1} and 0.38 Oe, respectively. The measured magnetic properties and the hysteresis behavior revealed the ferromagnetic activity of the $Cu_{0.5}Ni_{0.5}Fe_2O_4$@Lys-GO nanocomposite. The excellent ferromagnetic behavior of the $Cu_{0.5}Ni_{0.5}Fe_2O_4$@Lys-GO nanocomposite corroborated the magnetic segregation of the catalyst after the complete conversion of the tandem oxidative cyclization reaction, it is a far more efficient method than standard filtering or centrifugation[6].

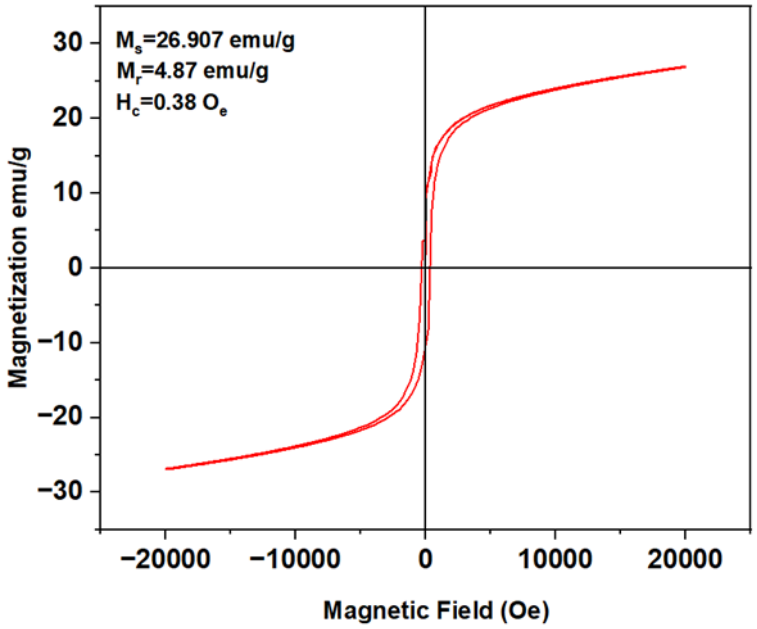

Figure S24. Magnetic hysteresis curve (M-H) for hysteresis curve (M-H) for $Cu_{0.5}Ni_{0.5}Fe_2O_4$@Lys-GO at 300 K.

Raman Spectroscopy.

The Raman spectra of Graphene oxide and $Cu_{0.5}Ni_{0.5}Fe_2O_4$@Lys-GO were recorded by Raman spectrometer equipment depicted in Figure S25. Substantially, there are multiple bands within the range of 1200 to 2800 cm^{-1} for substances based on carbon. The Raman spectra of substances based on graphene exhibited two prominent peaks, attributed to the first-order E2g mode from sp^2 carbon domains (G band), and characteristics of a breathing mode for k-point (D-band) are observed. Therefore, the electronic and phonon structure of the synthesized GO and $Cu_{0.5}Ni_{0.5}Fe_2O_4$@Lys-GO was examined utilizing Raman spectroscopy. The two prominent bands around 1308 cm^{-1} and 1584 cm^{-1} were observed because of the characteristic D and G bands of GO. Also, the Raman spectrum of $Cu_{0.5}Ni_{0.5}Fe_2O_4$@Lys–GO nanocomposite displays two strong peaks associated with the G–band and D–band, respectively at 1585 cm^{-1} and 1313 cm^{-1} [7].

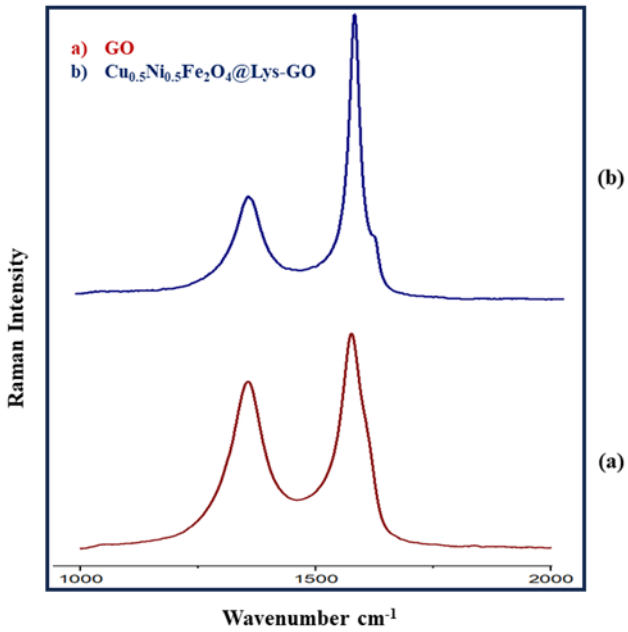

Figure S25. Raman spectra of GO (a) and $Cu_{0.5}Ni_{0.5}Fe_2O_4$@Lys-GO (b)

References

1. Nicol, A. W. In *Physicochemical Methods of Mineral Analysis*; Nicol, A. W., Ed.; Springer US: Boston, MA, **1975**; 249. DOI:10.1007/978-1-4684-2046-3_7.
2. Huang, H.-H.; De Silva, K. K. H.; Kumara, G. R. A.; Yoshimura, M. Sci. Rep. **2018**, *8*, 6849. DOI:10.1038/s41598-018-25194-1.
3. Khalaf, M. M.; Abd El-Lateef, H. M.; Alnajjar, A. O.; Mohamed, I. M. A. Sci. Rep. **2020**, *10*, 2761. DOI:10.1038/s41598-020-59655-3.
4. Arthi G, P. B.; Bd, L. J. Nanomedicine Nanotechnol. **2015**, *06*. DOI:10.4172/2157-7439.1000253.
5. J, B.; N, S.; R, J. Mater. Lett. **2012**, *81*, 52. DOI:10.1016/j.matlet.2012.04.076.
6. Anjana, V.; John, S.; Prakash, P.; Nair, A. M.; Nair, A. R.; Sambhudevan, S.; Shankar, B. IOP Conf. Ser. Mater. Sci. Eng. **2018**, *310*, 012024. DOI:10.1088/1757-899X/310/1/012024.
7. Lassoued, A.; Lassoued, M. S.; Karolak, F.; García-Granda, S.; Dkhil, B.; Ammar, S.; Gadri, A. J. Mater. Sci. Mater. Electron. **2017**, *28*, 18480. DOI:10.1007/s10854-017-7795-4.

